

# Simulation of the nanostructure evolution under irradiation in Fe-C alloys

V. Jansson<sup>a,b,\*</sup>, L. Malerba<sup>a</sup>

<sup>a</sup>*Institute of Nuclear Materials Science, SCK•CEN, Boeretang 200, 2400 MOL, BELGIUM*

<sup>b</sup>*Department of Physics, P.O. Box 43 (Pehr Kalms gata 2), FI-00014 UNIVERSITY OF HELSINKI, FINLAND*

## Abstract

Neutron irradiation induces in steels nanostructural changes, which are at the origin of the mechanical degradation that these materials experience during operation in nuclear power plants. Some of these effects can be studied by using as model alloy the iron-carbon system.

The Object Kinetic Monte Carlo technique has proven capable of simulating in a realistic and quantitatively reliable way a whole irradiation process. We have developed a model for simulating Fe-C systems using a physical description of the properties of vacancy and self-interstitial atom (SIA) clusters, based on a selection of the latest data from atomistic studies and other available experimental and theoretical work from the literature. Based on these data, the effect of carbon on radiation defect evolution has been largely understood in terms of formation of immobile complexes with vacancies that in turn act as traps for SIA clusters. It is found that this effect can be introduced using generic traps for SIA and vacancy clusters, with a binding energy that depends on the size of the clusters, also chosen on the basis on previously performed atomistic studies.

The model proved suitable to reproduce the results of low (<350 K) temperature neutron irradiation experiments, as well as the corresponding post-irradiation annealing up to 700 K, in terms of defect cluster densities and size distribution, when compared to available experimental data from the literature. The use of traps proved instrumental for our model.

**Keywords:** Fe-C alloys, Object Kinetic Monte Carlo

## 1. Introduction

Low alloy bannitic steels are used for the reactor pressure vessel (RPV) in most commercial nuclear power plants. Their integrity is the most important factor in the determination of the lifetime of a nuclear reactor. It is known that neutron irradiation causes hardening and reduction of the tensile elongation of these steels, leading to an increase of the ductile-brittle transition temperature (embrittlement) [1, 2, 3, 4]. For a full understanding of the degradation processes of steels, it is important to understand thoroughly how the nanostructure evolves under irradiation, *i.e.* how vacancies, SIA and their clusters interact with each other and with other impurities, such as interstitial carbon atoms.

Object Kinetic Monte Carlo (OKMC) is a stochastic

method that is adequate for simulating the nanostructure evolution in materials during irradiation or annealing. However, the method requires the pre-determination of the parameters that define the rate of events, such as migration of defects or dissociation of clusters, for all defects in the simulation. Since there are many kinds of defects, the properties of which usually vary with the size of the defect clusters, thousands of parameters are needed for a standard simulation. These may be obtained by using data from experiments, *ab initio* calculations and MD or other atomistic calculations. OKMC studies have been performed for Fe-systems *e.g.* by Domain *et al.* [5], but a good parameter set to simulate irradiation processes in Fe-C under any condition still needs to be elaborated.

Relatively few thoroughly reported and well-documented irradiation experiments on Fe-C systems can be found in the literature that are actually usable as reference for their simulation with the OKMC method

\*Corresponding author. Tel. +32 1433 3096, fax: +32 1432 1216.  
Email address: ville.b.c.jansson@gmail.com (V. Jansson)

[6]. We have chosen here two reference experiments: One irradiation experiment by Eldrup, Singh and Zinkle [4, 7] and one post-irradiation annihilation experiment by Eyre *et al.* [8]. The first of these experiments was chosen because of its completeness. The second one is in fact the only relatively well-documented post-irradiation annealing experiment on Fe that could be found. Low dose and relatively low irradiation temperature conditions have been chosen, because they involve less complexity when modelled with OKMC tools.

Eldrup *et al.* conducted an irradiation experiment on  $\alpha$ -Fe with about 80 atomic parts per million (appm) carbon and nitrogen at the High Flux Isotope Reactor (HFIR) at ORNL [7]. They estimate the neutron fluxes to be  $4 \cdot 10^{18}$  n/m<sup>2</sup>/s ( $E > 1$  MeV). The irradiation temperature was around 343 K. From the experiment, they report vacancy cluster number densities, obtained by positron annihilation spectroscopy (PAS) for different displacements per atoms (dpa) values, up to 0.23 dpa [7]. They also report the corresponding number densities of visible SIA clusters from transmission electron microscopy (TEM) studies of the same materials [4].

Eyre *et al.* irradiated specimens measuring  $76.2 \times 6.35$  mm at 333 K for three months up to 0.73 dpa in the DIDO reactor. The thermal and fission neutron doses were  $8.2 \cdot 10^{20}$  and  $2.5 \cdot 10^{20}$  n cm<sup>-2</sup>, respectively. The samples were afterwards annealed for 1 hour at various temperatures up to 773 K [8]. Using TEM, they measured the number densities of visible SIA clusters and their mean diameters at different temperatures.

To get a more complete picture from the available experimental data in  $\alpha$ -Fe, we have also considered other experiments, with less complete data: [9, 10, 11, 12, 13]. A more thorough overview of the available irradiation and annealing experiments with pure Fe will be published in a separate paper [6].

In this work, we develop an OKMC model that succeeds in simulating the defect evolution under irradiation and post-irradiation annealing of  $\alpha$ -Fe containing a certain amount of C. Key in our model is the identification of carbon-vacancy complexes as traps for SIA clusters, leading to a convincing understanding of the role of carbon on the nanostructural evolution of iron under irradiation. We will demonstrate the accuracy of our model by reproducing vacancy and SIA cluster density data from the above mentioned irradiation and annealing experiments. The paper is organized as follows: The OKMC method is described in section 2. Sec. 3 describes our set of parameters for SIA and vacancy clusters in Fe-

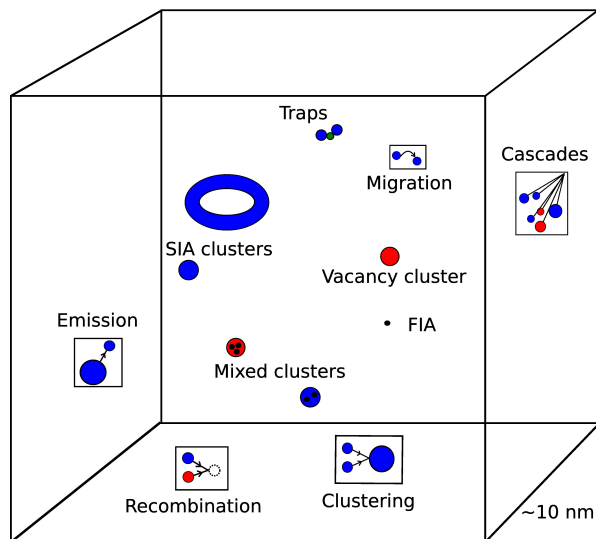


Figure 1: The OKMC simulation box with all objects and events used in our model.

C systems. In Sec. 4, we show simulation results under idealized conditions, for the purpose of parameterizing the traps that are used in the main model. The parameters for the traps are described in Sec. 5. In Sec. 6 and 7 are results from simulations of the nanostructure evolution under irradiation and annealing, respectively, using our main set of parameters. Finally, we discuss the results and present our conclusions.

## 2. Computation methods

For our OKMC simulations, we use the code LAKI-MOCA, which is already thoroughly described in [14]. In short, objects and possible events are introduced in a simulation box according to pre-defined probabilities (*Cf.* Fig. 1). Objects may represent vacancy and SIA clusters or any other nano- or microstructural feature. Every object has an associated reaction volume, that is generally spherically shaped (except for large dislocation loops, which have a toroidal shape). When the reaction volumes of two objects overlap, a predefined reaction, like clustering between two vacancy clusters or annihilation between a vacancy and an SIA, takes place.

The events in an OKMC simulation determine the dynamics of the system. The simplest event is one object migrating by one step (jump to first nearest neighbour distance), which is an example of an internal event. An external event is *e.g.* a cascade, which introduces new vacancy and SIA objects into the system. Common for

all events is that they have a probability that needs to be defined in the parameterization. In most cases these probabilities are expressed in terms of frequencies of thermally activated processes,

$$\Gamma_i = \nu_i \exp\left(\frac{-A_i}{k_B T}\right), \quad (1)$$

where  $\nu_i$  is the attempt frequency, alias the prefactor, for event  $i$ ,  $A_i$  is the corresponding activation energy,  $k_B$  is Boltzmann's constant and  $T$  the temperature. For every simulation step, an event is chosen, based on the corresponding probabilities in the parameterization, using the Monte Carlo algorithm [15]. When an event is selected, the progress in simulation time is calculated using the residence time algorithm [16].

A second kind of objects employed in our model are traps and sinks. Both have a spherical reaction volume with a radius that has to be specified. Both may act on vacancy clusters or SIA clusters, depending on their specification. When objects interact with a trap, they are bound to the trap by a certain trapping energy,  $E_t$ , specified for each kind of trap. We use traps to simulate the effect of carbon or carbon-vacancy complexes that are able to trap SIA clusters. When an object interacts with a sink, it is absorbed. Sinks are used to allow for the presence of dislocations in the material. Spherical sinks are used, the radius of which is defined in such a way that their sink strength equals the sink strength of dislocations. In addition, the presence of grain boundaries is allowed for, using the algorithm described in [17].

The foreign interstitial atoms, FIA, are another class of objects. FIA are a more explicit way to represent carbon, but also a more complex one, as more parameters have to be specified. Indeed, FIA may form mixed clusters with vacancy and SIA. These mixed objects need to have their own set of parameters as well.

LAKIMOCA can simulate damage production from electron, ion and neutron irradiation. In the case of electrons, Frankel pairs are introduced in the simulation box according to a certain dose rate, following the assumption that every electron produces one Frenkel pair. The pairs are introduced as uncorrelated pairs of single vacancy and SIA objects.

When simulating neutron (or ion) irradiation, debris of vacancy and SIA objects of different sizes are randomly introduced into the system at a certain rate per time and volume. The defect populations are chosen randomly from a database [18, 19, 20, 21, 22, 23] of displacement cascades simulated using molecular dynam-

ics (MD) with the Finnis-Sinclair potential [24]. The database contains cascades with energies of 5 keV, 10 keV, 20 keV, 30 keV, 40 keV, 50 keV and 100 keV. The accumulated dpa is calculated using the NRT formula [5, 25]:

$$dpa = \frac{0.8E_{MD}}{2E_D}, \quad (2)$$

where  $E_{MD}$  is the damage energy, *i.e.* the fraction of the kinetic energy of the primary knock-on atom (PKA) spectrum that is not absorbed by electronic excitation and is well approximated by the energy of the cascades in the MD simulations.  $E_D = 40$  eV is the displacement threshold energy for Fe.

We prefer to use a non-cubic simulation box in order to avoid anomalies from 1D-migrating defects entering a migration trajectory loop, due to the periodic boundary conditions, as discussed in [17].

### 3. Parameterization for SIA and vacancy clusters

The parameters needed to define the properties of point-defects and their clusters in our model are listed in Table 1. All parameters are in principle a function of the size of the defect clusters,  $N^\delta$  (where  $\delta = v$  denotes vacancies,  $\delta = i$  SIA and  $\delta = f$  FIA). To build these tables, we have gathered available data from *ab initio*, molecular dynamics, rate theory, atomistic and OKMC studies and carefully chosen the most accurate values to be used for our model. The chosen values for all parameters are described below for all species of objects, vacancies, SIA and traps.

The number of parameters needed is very large. However, it is important to emphasize that the goal of this work is to establish all physical parameters for which clear indications as to whether their values exist from fundamental studies or experiments, thereby limiting the need to calibrate only a few, if any, parameters, with clear physical interpretation. These, in turn, will be considered satisfactory if their value is physically acceptable.

#### 3.1. Vacancy clusters

In what follows, we describe in some detail how the numerical values of the parameters for vacancy-type defects were established.

Table 1: Overview of all parameters and their annotations:  $\delta = v$  for vacancies,  $\delta = i$  for SIA,  $\delta = f$  for FIA,  $\delta = fv$  for mixed FIA-vacancy clusters and  $\delta = fi$  for mixed FIA-SIA clusters.

$N^\delta$	-	The number of defects in the cluster — all parameters that follows are in principle functions of $N^\delta$ .
$\nu^\delta$	[s <sup>-1</sup> ]	The prefactor (or attempt frequency) for the cluster migration.
$M^\delta$	[eV]	The migration energy of the cluster.
$\nu_d^\delta$	[s <sup>-1</sup> ]	The prefactor (or attempt frequency) for a emission of a defect, $d = i, v$ or $f$ , from a cluster.
$M_d^\delta$	[eV]	The migration energy of a defect, $d$ , emitted from a cluster.
$B_d^\delta$	[eV]	The binding energy of a defect $d$ to a cluster
$r^\delta$	[Å]	The capture radius around a given spherical object, representing its strain field; when two spheres overlap the two objects react with each other
$\chi^\delta$	-	Parameter determining the shape of the object. If 1, the geometrical shape of the cluster is a torus, if 0, the shape is a sphere.
$\eta^\delta$	[eV]	The energy of rotation, used to define a pure probability (not frequency) of rotation of the Burgers vector associated with the cluster. A vanishing value corresponds to fully 3D motion, a value approaching 1 eV or more corresponds to fully 1D motion.
$E_t^\delta$	[eV]	The energy by which a defect $\delta$ is bound by a generic trap.

### 3.1.1. Diffusivity

The diffusion coefficient of a migrating species can be written equivalently as (see *e.g.* [26])

$$D(T) = D_0 \exp\left(\frac{-E_a^D}{k_B T}\right) = f_c(T) \frac{\Gamma(T) d_j^2}{2n}, \quad (3)$$

where  $D_0$  is the diffusivity prefactor,  $E_a^D$  is the diffusion activation energy,  $f_c$  ( $\sim 1$  in the case of three-dimensionally randomly migrating vacancy clusters) is the correlation factor (which may depend on the temperature),  $d_j$  is the single jump distance, and  $n$  is the dimensionality of the migration (1 for 1D migration, 3 for 3D migration). The jump frequency,  $\Gamma(T)$  is expressed as [26]:

$$\Gamma(T) = \nu^v \exp\left(\frac{-E_a^v}{k_B T}\right), \quad (4)$$

where  $\nu^v$  is the so-called attempt frequency. Assuming  $E_a^D \sim E_a^v$  (completely true in case of purely random walk; approximately true so long as correlated jumps remain rare events), one gets

$$D_0 \approx f_c \frac{\nu^v d_j^2}{2n} \approx \frac{\nu^v d_j^2}{2n}. \quad (5)$$

Therefore, neglecting correlation effects, the diffusivity is determined once attempt frequency and migration energy are known (if correlation effects exist, they must be introduced in the model separately) and these are the parameters that must be provided to LAKIMOCA in order to define the mobility of each migrating species.

*Attempt frequency for migration,  $\nu^v$ .* For the single vacancy, an attempt frequency of the order of the Debye frequency,  $\nu_1 = 6 \cdot 10^{12} \text{ s}^{-1}$  is used. The attempt frequency values given for the vacancy clusters will be expressed for convenience in terms of this value, used as a constant, which was fitted to the self-diffusion coefficient of iron at 300°C.

For clusters of size  $N^v = 2\text{--}250$ , values of attempt frequency obtained by atomistic KMC (AKMC) [27, 28] are used (*Cf.* Fig. 2. Missing values are interpolated using cubic spline. For  $N^v > 300$ , the clusters are assumed to migrate by surface diffusion mechanisms ([29], as in [30]):

$$\nu^v \sim \frac{\nu_1}{(N^v)^{4/3}}. \quad (6)$$

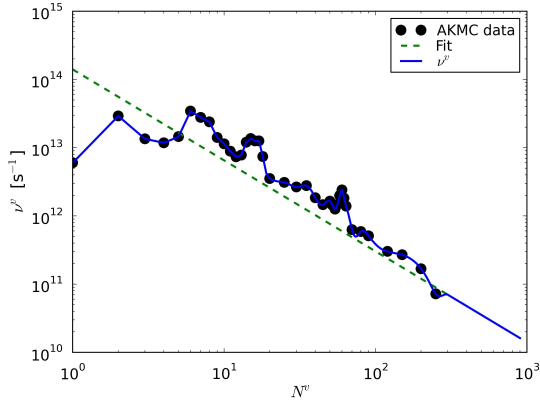


Figure 2: The attempt frequency parameterization,  $\nu^v$ , interpolated to AKMC data from [27, 28] and then extrapolated.

This scaling was smoothly joined to the AKMC values using the correlation:

$$\nu^v = -1.02064 \cdot 10^{-3} + \frac{1.410626 \cdot 10^{14}}{(N^v)^{4/3}}. \quad (7)$$

For clusters of sizes  $N^v = 251\text{--}299$ , the values are interpolated using cubic splines.

*Migration energy,  $M^v$ .* The migration energy for the single vacancy is taken to be 0.63 eV, as predicted by the Mendelev potential [31], one of the most reliable for radiation damage studies in iron. The reason for adopting the inter-atomic potential value instead of the experimental value or the one obtained from density functional theory is that the relative differences between migration rates are probably more important than the absolute values. Since the migration energies for clusters must necessarily be evaluated using the inter-atomic potential, for consistency, the inter-atomic potential value is also adopted in the case of the single vacancy. Density functional theory (DFT) calculations for the migration energy of the single vacancy give values between 0.64 eV [32] and 0.67 eV [33]; experimental values are reported to be 0.55 or 0.57 eV [34]. Mendelev’s potential gives 0.63 eV [31], which is sort of intermediate between experimental and DFT values. According to DFT, the di-vacancy has a migration energy similar to the single vacancy, whereas the tri-vacancy is more mobile [34]. This trend is respected by the values from [27], that we use.

For sizes  $N^v = 2\text{--}300$ , AKMC values [27] are used and

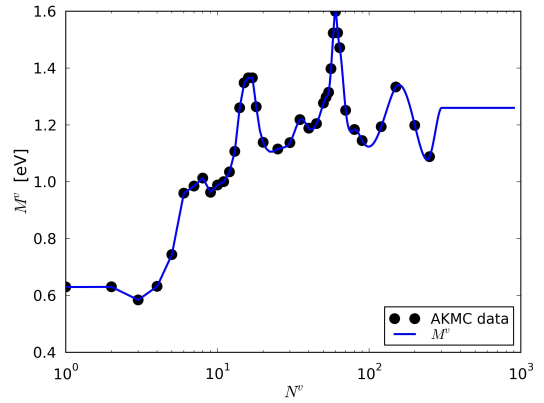


Figure 3: The migration energy for vacancy clusters,  $M^v$ ; interpolated to AKMC data from [27, 28] and then extrapolated.

the missing values are interpolated using cubic splines (Cf. Fig. 3. For  $N^v > 300$ , a single value is extrapolated from a smooth fit to the AKMC values, using only cluster sizes  $N^v > 10$ . Hence, the obtained migration energy for vacancy clusters of sizes larger than 300 vacancies is set to 1.26 eV. The dataset as a function of  $N^v$  is represented in Fig. 3. Note that the peaks that appear for  $N^v < 250$  have a physical explanation: they correspond to vacancy clusters in which a nearest neighbour shell is complete: due to their high symmetry, the surface motion of vacancies in these clusters is more difficult, hence the corresponding migration energy is higher [28].

### 3.1.2. Dissociation via emission of single vacancies

Dissociation via emission of clusters is an extremely unlikely event [28], so only single vacancy emission is considered. The dissociation (or emission) energy is by definition the sum of the migration energy of the emitted object plus its binding energy to the mother cluster:  $E_{diss} = B_v^v(N^v) + M_v^v(1)$ . Here, too, different series of values contribute to building the parameterization for all sizes.

*Jump frequency for emission,  $\nu_v^v$ .* In order to be consistent with the rate theory and guarantee that absorption and emission can reach steady state kinetic equilibrium—not to confuse with thermodynamic equilibrium—the vacancy emission must be proportional to the radius of the cavity, *i.e.* the power  $\frac{1}{3}$  of the

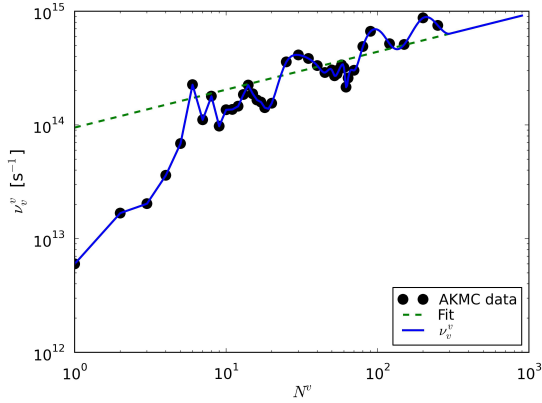


Figure 4: The attempt frequency for emission of a vacancy,  $\nu_v^v$ , from clusters of different sizes. The values are interpolated to AKMC data from [27, 28] and then extrapolated.

size expressed in terms of number of vacancies,  $N^v$ :

$$\nu_v^v \sim \nu_1 \sqrt[3]{N^v} \quad (8)$$

For  $N_v \leq 300$ , the parameters were again interpolated to AKMC values [27, 28] and then extrapolated with the function (Cf. Fig. 4):

$$\nu_v^v = -6.40388 \cdot 10^{-4} + 9.49849 \cdot 10^{13} \cdot \sqrt[3]{N^v}. \quad (9)$$

*Migration energy for emission of a single vacancy,  $M_v^v$ .* This energy is considered independent of the size of the mother cluster, so  $M_v^v = 0.63$  eV for all  $N^v$ .

*Binding energy,  $B^v$ .* The binding energy we refer to here is between the emitted single vacancy and the vacancy cluster.

For  $N^v \leq 300$ , we calculate  $B^v = E_{diss} - M_v^v$ , from the dissociation energies  $E_{diss}$ , obtained in [27, 28]. These values are lower than the binding energies statically calculated (either with the Mendelev potential or by DFT), because these are effective values that inherently take into account the fact that the configuration of the clusters keeps changing, thereby making dissociation easier than predicted based on the energy difference between the dissociated and the fundamental states of the cluster. In other words, these values include configurational entropy effects on the dissociation free energy. The missing values were interpolated using cubic splines. For

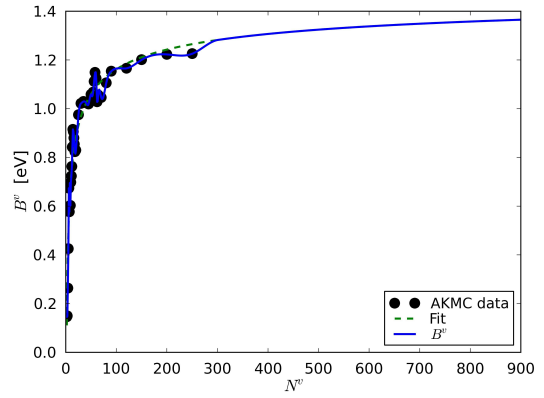


Figure 5: The binding energy of a vacancy to a cluster,  $B^v$ . The values are derived from dissociation energies, calculated with AKMC [27, 28] and then extrapolated. The asymptote of the extrapolated values is the formation energy of a vacancy according to the interatomic potential used..

$N^v > 300$ , the values were extrapolated by fitting the function,

$$B^v = 1.71 + 3.39716[(N^v)^{2/3} - (N^v + 1)^{2/3}], \quad (10)$$

to the AKMC values. This equation (10) interpolates fairly well the AKMC values up to  $N^v = 300$  and extrapolates them especially well, as is shown in Fig. 5—its asymptote is the formation energy of the vacancy according to the Mendelev potential, consistently with the fact that the emission of a vacancy from a very large voids is equivalent to creating a new vacancy in the bulk by removing an atom from a free surface.

### 3.1.3. Other parameters

*The capture radius,  $r^v$ .* Following Table 2 in [14]:

$$r^v = \frac{3.3a_0}{1 + \gamma} + \epsilon + a_0 \left( \frac{3}{8\pi} \right)^{1/3} \left( (N^v)^{1/3} - 1 \right) \quad (11)$$

with interstitial bias  $\gamma = 1.2$ ,  $\epsilon = 0.01$ , and  $a_0 = 2.87$  Å (the lattice parameter of iron). The rationale behind this expression is that the spherical volume associated with the cluster has a radius given by the radius of the cluster itself (second term, determined by how many vacancies are contained in it), increased by the range of the single defect strain field (first term), the latter obtained including the correction given by removing the radius of

the defects on the surface. The value  $3.3a_0$  corresponds to the distance at which recombination between interstitial and vacancy occurs in iron according to experiments (see refs. in [14]). The bias factor  $\gamma$  takes into account the larger strain field of self-interstitials, as compared to vacancies, and appears here in order to make sure that the recombination distance between SIA and vacancy is actually  $3.3a_0$  (see expression for SIA clusters below: the interaction distance is the sum of the capture radii of the two objects, *i.e.* interaction occurs when the two spheres associated with each object overlap).

*Loop nature,  $\chi^v$ .* In iron, at least under neutron irradiation, vacancy loop formation is not expected to be a frequent event, and the most stable clusters are “spherical”, so  $\chi^v = 0$  for all  $N^v$ .

### 3.2. SIA clusters

In what follows we describe in some detail how the numerical values of the parameters for SIA-type defects were established.

#### 3.2.1. Diffusivity

The theory is the same as for vacancies, *i.e.* it is summarised by Eqs. 3–5. Since SIA clusters migrate relatively fast, much faster than vacancy clusters, their diffusivity can be studied by MD. Reliable studies [35, 36] have been performed using Mendeleev’s potential [31], even though it does not reproduce correctly the stability of the non-parallel configurations of SIA clusters [37]. Because of the uncertainties concerning stability and mobility of non-parallel configurations, the actual parametrization will not reflect exactly the calculations. Moreover, as in the case of vacancies, it is justified to change some of the parameters to explore the importance of specific effects that the MD simulations cannot take into account (*e.g.* the effect of impurities). In particular, contrary to the case of vacancies, the migration energy of SIA clusters should not be considered as fully established.

*Migration attempt frequency,  $\nu^i$ , and migration energy,  $M^i$ .* For  $N^i \leq 7$ , the  $\nu^i$  and  $M^i$  values have been obtained with reference to Eq. 5, using as indication values from [35], slightly modified based on a series of considerations.

Overall there are three categories of migration energy values to be established, in different ways:

- Based on experiments [38], the migration energy of the single SIA in iron is 0.3 eV and the migration energy of the di-SIA is 0.4 eV, fully 3D in both cases. These values are also found in DFT [39], and the values obtained from dynamic simulations using Mendeleev’s potential in [35], namely 0.27 and 0.36, respectively, are also not dissimilar. The di-interstitial is actually more stable in a non-parallel configuration [37]; the unfauling energy, *i.e.* the energy required to switch from the non-parallel to the parallel configuration, was however estimated and found to be  $\sim 0.4$  eV from the interatomic potential, suggesting no difference as compared to the migration energy. In a DFT calculation [40] it was found that actually the non-parallel di-SIA, rather than unfauling, can migrate remaining in the same configuration, with an energy of  $\sim 0.55$  eV. However, here we shall adopt the more established value of 0.4 eV, which is supported by experiments.
- The migration energy to be used for clusters with 3–4 SIA should allow for the fact that these can only migrate when in parallel configurations (with relatively small energy, *i.e.* 0.14 eV and 0.15 eV, respectively [35]) but, according to DFT, will spend most time in non-parallel configurations; so, the bottleneck for migration becomes the unfauling process. The energy involved in the latter is not easy to estimate, because the available potentials predict the non-parallel configurations to be metastable, so dynamic simulations are not reliable, while static simulations require guessing all the steps of a process that, in the case of 3 and 4 SIA, can be fairly complex. It is, thus, a challenging calculation of uncertain outcome. In the case of the 4-SIA cluster, recently the unfauling energy seems to have been reliably estimated from Mendeleev’s potential to be  $\sim 0.8$  eV [41], so we shall adopt this as a reasonable value for its effective migration energy (a previous estimate [37] had provided 1.7 eV, which seems somewhat too high). In the case of the 3-SIA clusters the only estimate for the unfauling energy that is currently available is  $\sim 0.15$  eV, which was obtained from Mendeleev’s potential in [37]. This value is likely to be an underestimation, so we tentatively take for the 3-SIA cluster the same effective value of migration energy as for the di-interstitial,  $\sim 0.4$  eV.
- For the migration energy of large clusters ( $> 6$  SIA), which are assumed to migrate in 1D mainly, we take the value from MD,  $\sim 0.05$  eV (See *e.g.*

Table 2: The attempt frequencies,  $\nu^i$ , and the migration energies,  $M^i$ , for SIA cluster sizes of  $N^i = 1-7$ .

$N^i$	$\nu^i$ [ $10^{13} \text{ s}^{-1}$ ]	$M^i$ [eV]	
1	8.071	0.31	(Exp. value)
2	34.15	0.42	(DFT and exp. value)
3	1.175	0.42	
4	1.195	0.8	
5	0.156	0.1	
6	0.156	0.05	
7	0.171	0.05	

[36]). Alternatively, different choices can be made in parametric studies. However, we prefer to attribute the origin of the higher values found experimentally ( $\sim 1.3$  eV [42]) to the presence of impurities, so here we shall consider fixed the 0.05 eV value and will move to traps the responsibility of effectively changing this value. We have no data for the 5-SIA complex, so we use an intermediate value, 0.1 eV, to have a smoother transition from 0.8 eV for 4-SIA to the value of 0.05 eV for the 6-SIA complex.

Taking into account all these considerations, the parameters tentatively adopted for  $N^i \leq 7$  are shown in Table 2. Concerning the prefactors for  $N^i \geq 7$ , the following expression is used:

$$\nu^i = \frac{c}{(N^i)^{0.8}}, \quad (12)$$

Here,  $c$  is determined by requiring Eq. 12 to give the same values for  $N^i = 7$  as the values in the table above. Thus,  $c = 8.11 \cdot 10^{12}$ . The exponent of  $N^i$  in the denominator can theoretically vary between 0.5 (independent crowdion model) [43] and 1 (migration via kink pair formation along the edge of a loop) [44]. The value 0.8 adopted here respects the theory and corresponds to the value determined experimentally by Arakawa *et al.* [42].

### 3.2.2. Dissociation via emission of single SIA

The dissociation (or emission) energy,  $E_{diss}$ , is defined as the sum of the migration energy of the emitted object plus its binding energy to the mother cluster:  $E_{diss} = B_i^i(N^i) + M_i^i(1)$ . SIA clusters are known to be thermally highly stable, *i.e.* dissociation by emission of single SIA

is a very unlikely event, due to the strong binding energy. Therefore, *a priori*, any large enough value is acceptable and only small clusters (size 2–3) will actually have a small probability of emitting. For this reason, it is not really worth devoting specific studies to refine parameters in this case. However, recently binding energy values calculated using Mendeleev’s potential have become available and could therefore be used [45]. Here we take a simplified approach, as follows.

*Jump frequency for emission,  $\nu_i^i$ .* The jump frequency for emission is arbitrarily assumed to be the same as the one for the migration of the single vacancy and independent of the mother cluster size:

$$\nu_i^i = \nu_1 = 6 \cdot 10^{12} \text{ s}^{-1} \quad (13)$$

for all  $N^i$ .

*Migration energy for emission of a single SIA,  $M_i^i$ .* The migration energy for one SIA is simply chosen to be equal to the migration energy of the single interstitial, *i.e.*  $M_i^i = M^i = 0.3$  eV for all  $N^i$ .

*Binding energy,  $B_i^i$ .* The binding energy we refer to here is the one between the emitted single SIA and the SIA cluster. The simplest option is to use the formula reported *e.g.* in [14]. For  $N^i > 1$ :

$$B_i^i(N^i) = e_{for} + \frac{(B_i^i(2) - e_{for})((N^i)^s - (N^i - 1)^s)}{2^s - 1}, \quad (14)$$

where  $s = \frac{2}{3}$ ,  $B_i^i(2) = 1.0$  eV (binding energy of the di-interstitial); and  $e_{for} = 4.0$  eV (formation of the single interstitial).

### 3.2.3. Other parameters

*The capture radius,  $r^i$ , and the loop nature,  $\chi^i$ .* The capture radius for an SIA clusters is determined having in mind the fact that the SIA in the cluster are parallel to each other and distributed on a (111) plane, forming a platelet that can be approximated by a round disc for large enough sizes. The sphere associated with the cluster is assumed to be the one whose equatorial plane is the habit plane of the cluster, *i.e.* the disc associated, and whose equator is the edge of the loop. The capture radii are thus given by

$$r^i = r_0^i + \frac{a_0}{\sqrt{\pi} \sqrt{3}} (\sqrt{N^i} - 1), \quad (15)$$



$$r_0^i = \gamma \frac{3.3a_0}{1 + \gamma} \quad (16)$$

where  $\gamma = 1.2$  (interstitial bias) and  $a_0 = 2.87 \text{ \AA}$  is the lattice parameter of iron.

For large SIA clusters, we know that the strain field of a perfect dislocation loop is limited to a region surrounding the edge dislocation delimiting it, while a perfect lattice with no strain field is found at the centre of it. The shape of the strain fields of larger loops are thus better approximated by a torus. Tentatively, we assume that SIA clusters become loops when they exceed size 150. So, for  $1 < N^i < 150$ , the objects are spherical, denoted by  $\chi^i = 0$ , and for  $N^i \geq 150$ , they have toroidal form, denoted by  $\chi^i = 1$ . The major toroidal radius,  $R$ , is then given by

$$R = \sqrt{\frac{a_0^2 N^i}{\pi \sqrt{3}}}. \quad (17)$$

This expression comes from the assumption that the toroid is approximated by a circle with an area equal to  $N^i$  atomic areas. The minor toroidal radius,  $r = 7.215 \text{ \AA}$ , is given by Eq. 15 for  $N^i = 2$  for all sizes of toroidal SIA clusters.

*Dimensionality of migration,  $\eta^i$ .* Small clusters may flip their Burgers vector as a consequence of disturbances produced by impurities or simply as a spontaneous thermally activated process. The existence of non-parallel configurations and the possibility that, while migrating, the cluster turns into one of them can be an additional mechanism, because when unfauling, the Burgers vector may be different from the previous one. This effect is taken into account in the code by including a rotation energy from which a pure probability (not a frequency) is derived, in terms of a Boltzmann expression. A rotation energy  $\eta^i = 0$  produces changes of the Burgers vector (= jump direction) at each jump, thereby corresponding to fully 3D migration.  $\eta^i > 0$  reduces the chances of changing direction at each jump, so that the defect changes jump direction only after a number of 1D jumps. Values of  $\eta^i$  in excess of 1 eV provide almost fully 1D migration (depending on the temperature).

Precise information about the values of  $\eta^i$  and the actual dimensionality of the migration of the different clusters is not available, but it is known that there is a transition from fully 3D to fully 1D migration with increasing size. We use  $\eta^i = 0$  for single and di-interstitials and increase the value gradually to 1 eV for larger sizes.

### 3.3. Treatment of grain boundaries and dislocations

Grain boundaries and dislocations are sinks for both SIA and vacancies. In LAKIMOCA, a defect is removed when it has travelled farther than the length of the average grain size [14].

Dislocations are here assumed to be sinks only for small defects. As the dislocation density in the material by Eldrup *et al.* [7] is very low,  $\rho_d = 10^{12} \text{ m}^{-2}$ , by applying the equivalence with spherical sinks [46], *i.e.*

$$k_s^2 = 4\pi r_s n_s = \rho_d, \quad (18)$$

we found that  $r_s$ , the radius of the sphere, has a very small value, assuming that the number density of spherical sinks,  $n_s$  to be 1 sink in the system. As a consequence, the influence of the dislocation bias on the results of the model cannot be assessed when comparing with this reference experiment.

## 4. Study of populations of small C-V complexes

In this section we report the results of a study of post-irradiation annealing performed under ideal conditions. Namely, we consider only vacancies and FIA (C atoms). The purpose of this study is to have an idea of which C-V complexes should be expected to form in majority after irradiation at  $< 370 \text{ K}$  and how the population of complexes would change upon annealing up to above  $600 \text{ K}$ . This study is then used as guideline for the parameterization of traps, described in section 5. For the sake of simplicity, we restricted the degrees of freedom of the system by only allowing  $V_1$ ,  $V_2$ , C, CV,  $CV_2$  and  $C_2V$  complexes to be stable, as it makes it possible to compile a complete parameter set based on available data, without any need for fitting. Moreover, indications from interatomic potentials seem to suggest that larger complexes might not be especially stable, although uncertainties remain in this respect [47]. The parameters used for this specific simulation are described in the next section.

### 4.1. Parameterization with explicit C objects

For vacancies, the same parameters were used as described before in Sec. 3.1, except that the migration energy for emission is set to  $M_v^v = 0.0$  for vacancy objects with more than two vacancies ( $N^v > 2$ ), in order not to form voids and focus the attention on the relative fraction of small C-V complexes, which are expected to be the most common.

Table 3: The parameters for the FIA and vacancy-FIA objects for the study of populations of small C-V complexes. Only  $V_1$ ,  $V_2$ , C, CV,  $CV_2$  and  $C_2V$  are allowed. The parameters make all other complexes unstable by putting the binding energy  $B_v^{fv} = 0$ .  $\nu^{fv} = \nu_f^{fv} = \nu_v^{fv} = 6.0 \cdot 10^{12} \text{ s}^{-1}$ ,  $M^{fv} = \infty$ ,  $M_f^{fv} = 0.902 \text{ eV}$  [48] and  $M_v^{fv} = 0.63 \text{ eV}$  for all  $N^f$  and  $N^v$ .

Complex	$N^f$	$N^v$	$B_f^{fv}$ [eV]	$B_v^{fv}$ [eV]
CV	1	1	0.64 [49]	0.64 [49]
$CV_2$	1	2	1.01 [50]	0.49 [49]
$CV_3$	1	3	0.93 [50]	0.0
$CV_4$	1	4	0.96 [50]	0.0
$CV_5$	1	5	0.23 [50]	0.0
$CV_6$	1	6	1.20 [50]	0.0
$CV_n$	1	$7 \leq$	1.20	0.0
$C_2V$	2	1	1.01 [49]	2.3 [49]
$C_2V_2$	2	2	1.18 [49]	0.0
$C_2V_3$	2	3	0.93	0.0
$C_2V_4$	2	4	1.01	0.0
$C_2V_5$	2	5	1.23	0.0
$C_2V_6$	2	6	1.30	0.0
$C_2V_n$	2	$7 \leq$	1.30	0.0
$C_3V$	3	1	0.00	2.3
$C_3V_2$	3	2	0.00	0.0
$C_3V_n$	3	$3 \leq$	0.00	0.0
$C_4V$	4	1	0.00	2.3
$C_4V_2$	4	2	0.00	0.0
$C_4V_n$	4	$3 \leq$	0.00	0.0

For single carbon, the attempt frequency is set to the standard value  $\nu^f = \nu^1 = 6 \cdot 10^{12} \text{ s}^{-1}$  and the migration energy to  $M^f = 0.90 \text{ eV}$  [48]. The capture radius is set to  $5.0 \text{ \AA}$ . Complexes of only carbon are forbidden by making them immobile, with a very high migration energy  $M^f \geq 10.0 \text{ eV}$ , and unstable, with a binding energy of a carbon atom to the cluster,  $B_f^f = 0.0$ , for complexes with more than one carbon,  $N^f > 1$ . The parameters for mixed C-V clusters are shown in Table 3.

#### 4.2. Results

We introduced a random population of carbon in a simulation box of size  $150 \times 200 \times 250 \times a_0^3$ . We included dislocations as sinks in a similar way to what was described in Sec. 3.3. We also used a grain size of  $33 \mu\text{m}$ .

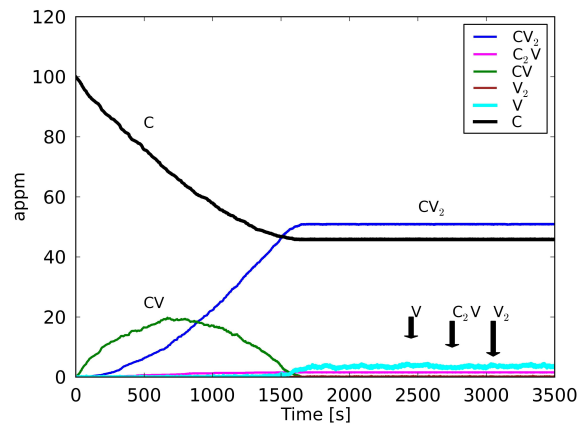
The irradiation of the system at 333 K was simulated by a constant flux of one vacancy per second. As the system could possibly behave very differently if it contains more vacancies than C atoms, or if the populations are more equal, we used one case where a number of vacancies were systematically removed continuously (by artificially disappearing at grain boundaries, beyond the correct sink strength) and one case where they were not. The evolution of the density of the different complexes is shown for both regimes in Fig. 6. Both systems reach a steady state, regarding the C-V complexes. In the system with low amount of vacancies (in the end an equal amount of C and V remains), the steady state is reached faster and not all C atoms are bounded to vacancies. In the final state, the number of  $CV_2$  complexes is 32 times higher than the number of  $C_2V$ . The CV complexes have disappeared completely by becoming  $C_2V$ . In the case with high amount of V (in the end twice as many V as C), all C are bounded to V and the level of  $CV_2$  is about ten times higher than the density of  $C_2V$ .

The previously irradiated systems were then annealed by raising the temperature by steps of 50 K, keeping the system at each temperature for one hour. The evolution of the density of the complexes is presented in Fig. 7. It is observed that  $CV_2$  complexes are dominating at low temperature, below 480 K, whereas the  $C_2V$  complexes dominate at higher temperatures for both cases. The major difference between the two regimes is the absence of free C in the system with high amount of V.

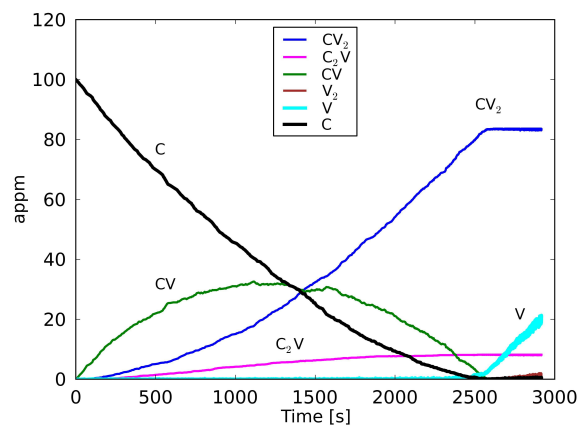
### 5. Parameters for the effect of carbon

Foreign interstitial atom (FIA) objects are the most explicit way of describing carbon, but because of the formidable complexity in terms of parameters that are added by the complexes it forms with point-defect clusters, we used them only in Sec. 4. In this section, we describe the parameters for the traps that translate the effect of C and which, together with the set of parameters for SIA and vacancies, described in Sec. 3, will form the full model. The traps represent not only single C atoms, but also small carbon-vacancy clusters, such as CV,  $CV_2$  and  $C_2V$ . The latter complexes bind strongly enough to SIA clusters to be able to trap them. The traps are essential for the simulations to reproduce the experimental data.

CV,  $CV_2$  and  $C_2V$  complexes have been found to be highly stable by MD simulations [47] and in particular the  $C_2V$  complex is stable up to 700 K. There is also ample experimental evidence of the existence of

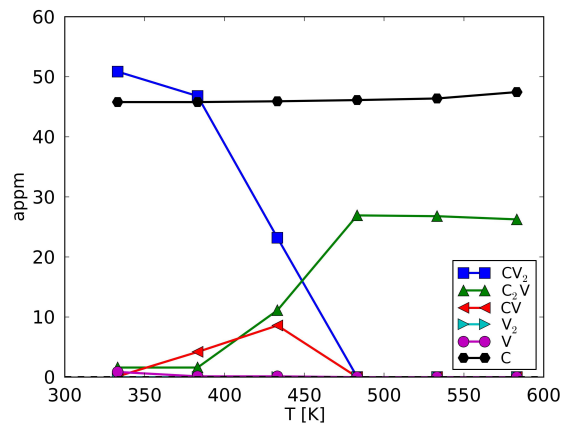


(a)

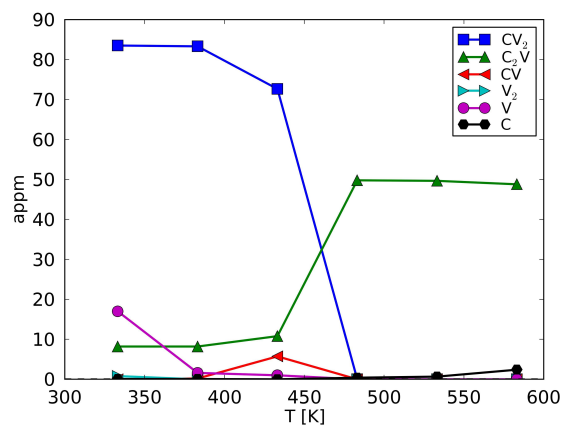


(b)

Figure 6: The evolution of a carbon-dominated (a) and a vacancy-dominated system (b) with small C-V complexes and under irradiation.



(a)



(b)

Figure 7: Annealing of the small complex carbon-dominated (a) and vacancy-dominated (b) system to obtain the temperature dependence.

Table 4: Binding energies between C-V complexes and the edge or the centre of large SIA clusters (size 61 SIA), according to MD simulations [51].

	SIA binding energy [eV]	
	Centre	Edge
C	0.0	0.6 [47]
CV	0.3	0.75
CV <sub>2</sub>	1.4	0.8
C <sub>2</sub> V	0.4	1.4–1.5

these complexes, as reviewed in [6]. MD simulations by N. Anento and A. Serra [51] show that C-V complexes bind to  $1/2\langle 111 \rangle$  SIA clusters with different binding energy, depending on whether the complex is interacting with the edge or the centre of the SIA cluster. At the edge, the vacancies in the complex tend to recombine, whereas this does not happen at the centre. The binding energies for C-V complexes with  $1/2\langle 111 \rangle$  SIA clusters according to MD simulations are given in Table 4. It can be seen that CV<sub>2</sub> and C<sub>2</sub>V are particularly strong traps for SIA clusters, depending on the point of interaction and the temperature. CV<sub>2</sub> is a strong trap if it interacts with the centre of the SIA cluster, but weak if interacting with the edge. All complexes with only one C are weak traps if interacting with the edge as the V will recombine. CV<sub>2</sub> is a strong trap only if it interacts with the centre.

We use generic spherical traps to simulate not only the formation of C-V complexes, but also their interaction with SIA clusters. Gyeong-Geun Lee *et al.* [52] noted that it is crucial that the efficiency of the SIA traps depends on the size of the trapped SIA cluster, as the SIA clusters otherwise tend to merge together until only a single large SIA cluster is left in the simulation box, independently of the size of the simulation box. To obtain this dependency, Lee *et al.* used a dissociation rate that was proportional to  $(N^i)^{-1}$  or  $(N^i)^{-2}$ . Here, we adopted a method where we specify the trapping energy  $E_t^i$  explicitly for all sizes, including temperature dependence when necessary. In Table 5 the trapping energies for SIA and vacancy clusters up to size 6 are presented.

For simulations at low temperature, 330–480 K, the sizes of SIA clusters may be divided into three categories, in order to define their trapping energy. For size 1–4, we use DFT data for the binding energy between a C atom and an SIA cluster, according to [50]. From size 5 to the threshold size,  $N_{th}$ , we use the value of the binding energy for a C atom to a SIA cluster, 0.6 eV [47].

Table 5: The trapping energies for the SIA traps. The SIA values for sizes 1–4 and the vacancy values for sizes 1–6 are from DFT calculations [50].

$N^i$	SIA $E_t^i$ [eV]	Vac. $E_t^v$ [eV]
1	0.17	0.65
2	0.28	1.01
3	0.36	0.93
4	0.34	0.96
5	0.60	1.23
6	0.60	1.20

This value is the same whether the cluster interacts with a single C atom or a CV<sub>2</sub> complex, which is the dominating trap in this range of temperatures. Indeed, for clusters sufficiently small, the highest chance is that the interaction occurs with the edge, leading to recombination of the vacancy and interaction energy with single C, *i.e.* 0.6 eV. Above size  $N_{th}$ , in the third category, we use a strong binding energy, 1.2 eV, that can be associated to the CV<sub>2</sub> complex bound to the centre of the SIA, and comparable to MD results in [51]. The threshold,  $N_{th}$ , is used as a calibration parameter, that effectively takes into account the probabilities for three different interactions with a SIA cluster at 330–480 K: the strong interaction of CV<sub>2</sub> complex with the centre, the weak interaction of ditto complex with the centre or the weak interaction of a single C with an SIA cluster.

For temperature of 480–680 K, we assume that the dominating strong traps are C<sub>2</sub>V (*Cf.* Sec. 4) and we therefore fitted the  $E_t^i$  for SIA clusters of sizes above  $N_{th}$  to 1.4 eV, consistently with the calculations in [51]. For temperatures above 680 K, we assume that the C<sub>2</sub>V complexes begin to dissociate, leaving only single C atoms in the system, with  $E_t^i = 0.6$  eV.

In the case of vacancy clusters, we use the same trapping energies for vacancies,  $E_t^v$ , for all temperatures. For  $N^v = 1–6$ , we use DFT values from [50]. For  $N^v > 6$ , we assume no trapping, as suggested by [47, 53].

## 6. Simulation of the nanostructure evolution under irradiation

We simulated an irradiation experiment with the setup used by Eldrup *et al.* in [7]. The irradiation temperature was 343 K and the simulation box size was  $350 \times 400 \times 450 \times a_0^3$ . Periodic boundaries were used in

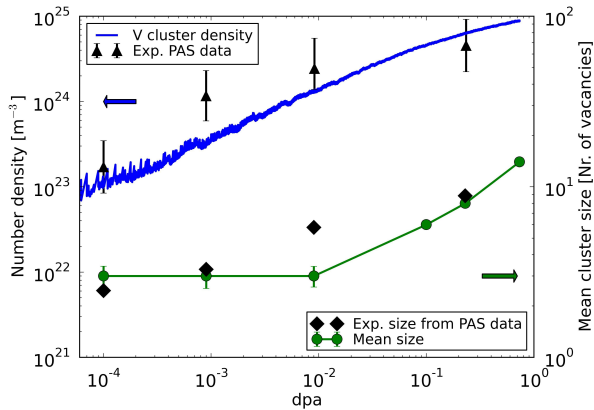


Figure 8: The vacancy cluster number density and mean size evolution versus dpa for the best case. The experimental data are from [7].

three dimensions. Cascades were introduced with a rate equivalent to  $7 \cdot 10^{-7}$  dpa/s. As either SIA or vacancy objects can be exclusively trapped, two populations of 100 appm traps were employed to include the effect of C on vacancies and C-V complexes on SIA clusters. The trapping energy depends on the size of the trapped object, as in Table 5. Two spherical absorbers for SIA and vacancies, respectively, were introduced as sinks equivalent to a dislocation density of  $10^{12} \text{ m}^{-2}$ . The grain size was  $33 \mu\text{m}$ . The simulation was stopped when 0.734 dpa had accumulated.

The vacancy cluster number density and mean size versus dpa, as compared to experimental data, are shown in Fig. 8 for the best case, *i.e.*  $N_{th} = 29$  (see below for more details). The corresponding size distribution of vacancy clusters for different doses is shown in Fig. 9. The results of the simulation show good agreement with the experimental data.

The density of visible SIA clusters ( $N^i > 50$ ) versus dose is shown in Fig. 10, and compared with a number of experimental data from TEM examinations of irradiated Fe-C alloys. The threshold,  $N_{th}$ , was fitted to the TEM data from Zinkle and Singh, denoted as triangles in Fig. 10. The best fit was obtained, in this case, with  $N_{th} = 29$ . The results for  $N_{th} = 27$  and 31 are also shown and suggest that a higher  $N_{th}$  gives a lower visible SIA cluster density. Values of  $\sim 30$  seem indeed reasonable as threshold above which complexes would mainly interact with the centre of the loop and changing the value allows one to remain within the experimental range. Another way of comparing the evolution of SIA

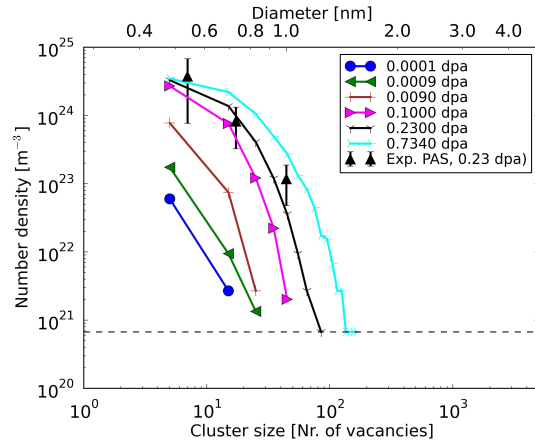


Figure 9: The vacancy cluster size distribution for different doses for the best case. The size increment is by 10 vacancies. The dotted line gives the density for one defect in the simulation box. The experimental data for 0.23 dpa (triangles) are from [7].

clusters with experiments is to consider the dislocation density due to loops, as shown in Fig. 11 for  $N_{th} = 29$ . One advantage of this choice is that the scatter of data from different experiments is significantly reduced. The agreement is good (in both cases) starting from  $10^{-3}$ – $10^{-2}$  dpa, but the model underestimates by an order of magnitude the dose at which SIA clusters become visible.

The mean cluster size at different doses is shown in Fig. 12. The mean sizes are overestimated compared to the reported experimental data [4], although the trend is correct. The evolution of the size distribution of SIA clusters versus dpa is shown in Fig. 13.

## 7. Simulation of the nanostructure evolution during isochronal annealing

We simulated a complete post-irradiation-annealing experiment in a box of size  $350 \times 400 \times 450 \times a_0^3$ . In the reference experiment [8], iron was irradiated at 333 K at 0.37 dpa at a dpa rate of  $5 \cdot 10^{-8}$  dpa/s. Similarly to the previous case, we introduced 100 appm traps for SIA objects, as well as 100 appm traps for vacancy objects. The traps, that we assume are representing C and CV and  $CV_2$  at low temperatures, had the same defect-size-dependent and temperature-dependent-binding energies as described in Sec. 5 and in Table 5. No values for the dislocation density and grain sizes are reported in [8].

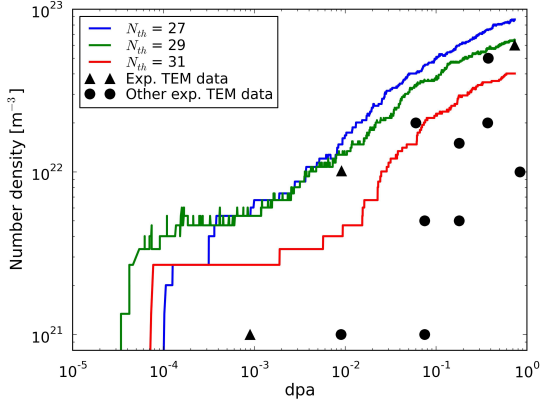


Figure 10: Number density of visible SIA versus dpa.  $N_{th} = 29$  corresponds to our best case. The reference experimental data are denoted with triangles [4]. Included in the graph are also data from other comparable irradiation experiments in Fe-C (bullets) [9, 8, 10, 11, 12, 13]. See [6] for full details.

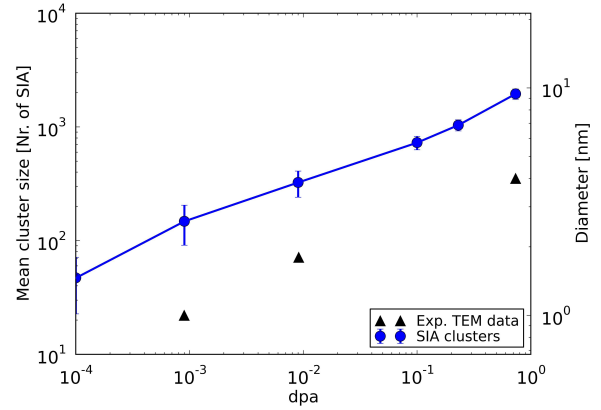


Figure 12: The SIA cluster mean sizes and their standard deviations for different dpa. The experimental data are from [4].

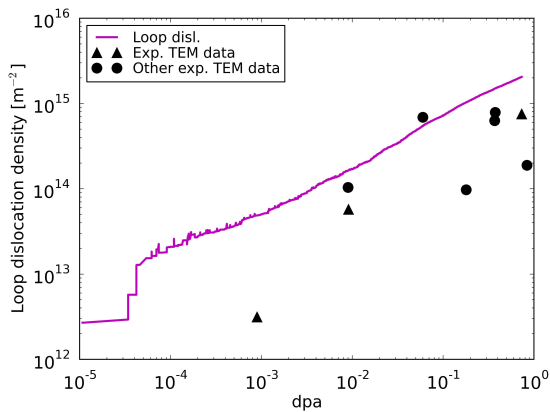


Figure 11: Loop dislocation density versus dpa. The reference experimental data are marked with triangles [4]. Included in the graph are also data from other comparable irradiation experiments in Fe-C (bullets) [9, 8, 11, 12, 13]. See [6] for further details.

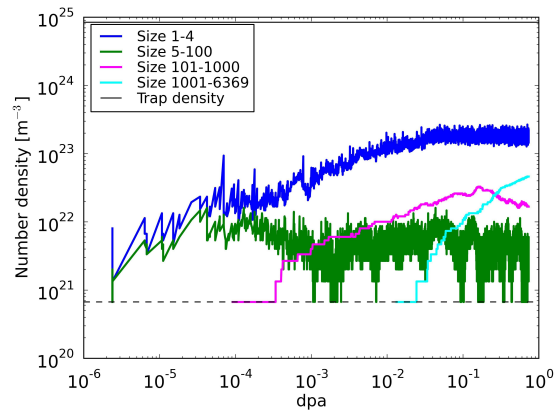


Figure 13: The SIA cluster size distribution evolution as function of dpa. The dotted line gives the density for one defect in the simulation box.

We used the same values as in the previous simulation in Sec. 6

After irradiation the system underwent isochronal annealing, where the temperature was increased by 50 K after every hour (3600 s), until a final temperature of 733 K was reached. We simulated the evolution with temperature and traced the number density of visible SIA clusters, as well as the number of SIA in visible clusters (SVC), as shown in Fig. 14 to compare with corresponding experimental data.

Before the temperature was raised to 483 K, we assumed that carbon atoms should have become mobile and thus able to form the stronger  $C_2V$  traps, as is suggested by the study performed in Sec. 4.2 (Fig. 7). We thus raised the trapping energy for large SIA (larger than  $N_{th}$ ) to different values,  $E_t^i = 1.3, 1.4$  and  $1.5$  eV. According to MD simulations the binding energy between a SIA cluster and a  $C_2V$  complex is  $1.4\text{--}1.5$  eV [51]. Our results indeed suggest a value between  $1.4$  and  $1.5$  eV for  $E_t^i$ . The trapping energies of the vacancy traps were unchanged, but their number was correspondingly reduced by 50%.

Using the *ab initio* values for the  $C_2V$  complex from Table 3, the dissociation energy can be calculated as  $E_{diss} = M_f^{fv} + B_f^{fv} = 1.90$  eV, which, using the formula for thermally activated events,

$$\Gamma_e = \nu^{fv} \exp\left(\frac{-E_{diss}}{k_B T}\right) \quad (19)$$

gives an average lifetime of the complex,  $\Gamma_e^{-1} = 18.4$  s, at  $T = 683$  K, rendering the complex unstable. Above this temperature, we can thus assume only C atoms to remain in the box, all C-V complexes being dissolved. Thus, before the temperature was raised to 733 K, we lowered the trapping energy for large SIA clusters to  $0.6$  eV, *i.e.* the binding energy between C and large SIA clusters [47]. The number of traps were again raised by 50 % to the original density. Due to the lowered trapping energy all SIA and vacancy clusters disappear, mostly due to recombination (in the absence of other efficient sinks). This is also seen in the experimental data. If the trapping energy is not lowered, with  $E_t^i = 1.4$  or  $1.5$  eV, some SIA clusters will remain longer in the box than the experimental data show. With  $E_t^i < 1.4$  eV the clusters disappeared too fast.

We also did a separate study where we kept the pre-irradiated system at the constant room temperature of 290 K to see if any changes could be expected from normal storage of the irradiated material. While the va-

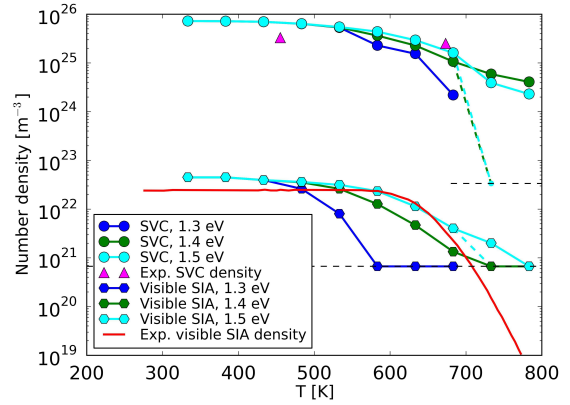


Figure 14: The density of visible SIA clusters and SIA in visible clusters (SVC) as a function of temperature during the simulated isochronal annealing. Different trapping energy for SIA,  $E_t^i = 1.2\text{--}1.5$  eV, are used at the temperature of 483 K and higher. Above 733 K, if the trapping energy was decreased to  $E_t^i = 0.6$  eV, all clusters disappear, as indicated by the dashed coloured lines. The solid line and the triangular dots are the experimental visible SIA cluster density and the SVC density, respectively, from [8]. The latter points are calculated from the reported visible SIA densities and the cluster diameter data. The dotted black lines indicates the density corresponding to one object in the box (lower line) and the minimum SVC simulation resolution (higher line), respectively.



cancy and SIA densities dropped a bit and the mean cluster sizes rose a bit, no significant changes could be observed after a simulation time of about one year.

## 8. Discussion

### 8.1. Small C-V complexes

The study of small C-V complexes in Sec. 4 has inherent limitations as the formation of large V and C-V complexes is deliberately forbidden, while SIA are altogether absent. Still, as steady-state is reached after a relatively short time and  $\sim 10^{-4}$  dpa, it can be assumed that the same steady-state would be reached very quickly in a real irradiation, before the SIA cluster population starts to build up. In this sense, the use of traps instead of the more cumbersome explicit treatment of all possible C-V clusters is acceptable.

We used two regimes, where one was under-saturated and the other was over-saturated with vacancies. The second one might look closer to a real irradiation but in reality whether one regime or the other is correct it will depend on the actual C content in the matrix and on the efficiency of the sinks. The two regimes can be considered as representative limiting cases. Concerning the density of  $CV_2$ , both regimes are characterised by more or less the same behaviour. The main difference is that in the under-saturated regime, there is an abundance of free C, whereas in the over-saturated regime there is not, as they are all bound to  $CV_2$  after the irradiation. In Sec. 4.2, we clearly see that  $CV_2$  is the dominating complex at the irradiation temperature chosen in this work, especially if we disregard the weakly trapping C atoms. This is logical as C atoms at low temperatures are virtually immobile and V have more time to bind to C defects.

Based on the parameters deduced from *ab initio* data, above 480 K, C is mobile and will join with the  $CV_2$  complexes, creating the  $C_2V$  complexes, as the second V becomes weakly bound in the  $C_2V_2$  complexes and is quickly emitted. As there can be a difference of 0.6–1.0 eV for the binding energy of a  $C_2V$  and a  $CV_2$  complex to the same point of a SIA cluster (centre or edge) [51], there are clearly two different regimes for SIA traps at lower and higher temperatures, respectively.

### 8.2. Cluster evolution under irradiation

Sec. 6 demonstrates that our model correctly reproduces the vacancy density cluster evolution under irradiation

at 343 K. For the SIA clusters, we compare the simulation data in two ways with the available experimental data: in terms of density of visible loops, and in terms of loop dislocation density, as functions of dpa. As all the experimental data are retrieved from TEM studies, which we expect to have fairly large error bars, up to about one order of magnitude, we can say that we have good agreement also for the SIA evolutions, comparing specifically to the data by Zinkle and Singh [4], to which the visible SIA density was in fact fitted by varying the threshold parameter,  $N_{th}$ , (the only fitting parameter used here). The other TEM data show a rather extensive scatter, illustrating the large experimental uncertainties. It can be noted that the newer experiments (our reference experiment is the most recent one) tend to have higher densities than the older ones, which might be explained by the higher resolution of newer electron microscopes.

The SIA mean cluster sizes are systematically larger, compare to the experimental data by S.J. Zinkle and B.N. Singh [4], but their reported mean sizes are on the other hand surprisingly small, down to  $\sim 1$  nm in diameter, (they report a TEM resolution of 0.5 nm, which is a significantly smaller than the more standard value of 1.5 nm, which we indeed have used as a lower size limit for visible clusters). A lower value of the limit for visibility in the analysis for the simulation data does not improve our results, though the experimental data might thus in fact be a bit underestimated in case of the mean size.

The defect size dependence of the trapping energy to the SIA traps proved crucial for the model. With a constant trapping energy for all sizes, all SIA clusters would eventually merge together to a single large cluster, at high enough dpa. This would happen independently of the simulation box size, which is not physical. The importance of a size dependence of the emission rate from traps was already evidenced in [52], however here we provide a physical interpretation for it, in terms of changing dominant mechanism in the interaction between C-V complexes and SIA clusters (edge versus central interaction).

### 8.3. Post-irradiation annealing

To be successful, the simulation of the isochronal annealing in Sec. 7, had to be divided into three different temperature ranges where the trapping energy changed according to the results from Sec. 4. In particular, the trapping energy,  $E_t^i$ , for large SIA clusters above the threshold size,  $N_{th}$  was changed from the first to the second stage to agree with the values attributable to the

dominant C-V cluster species, *i.e.* from  $E_t^i \sim 1.2$  eV for  $CV_2$  to 1.4 eV for  $C_2V$ . 1.2 eV is enough to completely trap SIA clusters at the first stage, but not enough at the higher temperatures at the second stage ( $>483$  K), why the stronger value of 1.4 eV of the  $C_2V$  [51] complex is necessary. Indeed, the MD study by N. Anento and A. Serra suggests that the binding energy of  $CV_2$  should be 1.4 eV as well [51], which is still in good agreement with our results, as a higher trapping energy at the first stage does not change anything.

In the third stage, the weak traps, corresponding to isolated C atoms, interact very little with the large remaining SIA clusters, but still prevent them to all cluster together into a single cluster. In the end all clusters either recombined or were absorbed by the grain boundaries or other sinks.

The overall temperature evolution shows fair agreement for all three stages of the annealing with the experimental data for both the visible SIA density, as well as SIA in visible clusters.

#### 8.4. General discussion

Clearly, the present model has limitations related to the fact that the physics of the formation of complexes between C atoms and point-defects, vacancies but also SIA clusters, is implicit in the parameterization of the trapping energies. A more evolved model should include explicitly all the ingredients and provide spontaneously all the effects. Yet, it is believed that the present work represents a significant step forward towards the development of nanostructural models for Fe alloys, including steels, by providing a reference for the elaboration of more complete ones.

An issue that was not addressed here concerns the sensitivity of the model to the variation of key parameters on which uncertainties remain, first of all the SIA cluster threshold size explicitly used to fit the results. Moreover, it is of high interest to perform a wide exploration on the effect of irradiation parameters such as flux. These studies have actually been performed; however, because of the extensive amount of results they led to, it has been preferred to report them in a separate paper [54].

## 9. Conclusions

We have presented an OKMC model based on the use of a physically fully motivated parameter set, which succeeds in describing the nanostructure evolution in Fe-C

systems under irradiation at 333–343 K ( $<100^\circ\text{C}$ ) and during post-irradiation annealing.

Key for the success of the model is the deep understanding, based on *ab initio* and interatomic potential calculations, of the interaction between C atoms and point-defects, to form stable complexes with vacancies that are in turn capable of binding migrating SIA clusters. In this paper the physics is simplified by introducing appropriately parameterized traps for point-defect clusters, following the example of previous models. Next step will be the implementation of a full set of parameters treating explicitly the formation of complexes involving C.

## Acknowledgement

This work was carried out as part of the PERFORM60 project of the 7th Euratom Framework Programme, partially supported by the European Commission, Grant agreement number FP7-232612. The authors wish to thank N. Anento, C. Becquart, A. De Baker, C. Domain, A. Serra, and D. Terentyev for advice, assistance and fruitful discussions during the performance of this work.

## References

- [1] E. Little, *International Materials Reviews*, 21 25 (1976) 36.
- [2] G. Odette, G. Lucas, *Radiation effects and defects in solids* 144 (1998) 189–231.
- [3] G. Odette, G. Lucas, *JOM Journal of the Minerals, Metals and Materials Society* 53 (2001) 18–22.
- [4] S. Zinkle, B. Singh, *Journal of Nuclear Materials* 351 (2006) 269–284.
- [5] C. Domain, C. Becquart, L. Malerba, in: N. Ghoniem (Ed.), *Proceedings of Second International Conference on Multiscale Materials Modeling: October 11 - 15, 2004, Los Angeles, California, Mechanical and Aerospace Engineering Department, University of Calif., 2004.*
- [6] L. Malerba, *Experimental reference cases for model validation in Fe and FeC alloys*, Technical Report, Public Deliverable Nr. D1-3.10, FP7/Perform60 Collaborative Project, Grant Agreement Nr. FP7-232612, 2011.
- [7] M. Eldrup, B. Singh, S. Zinkle, T. Byun, K. Farrell, *Journal of Nuclear Materials* 307 (2002) 912–917.
- [8] B. Eyre, A. Bartlett, *Philosophical Magazine* 12 (1965) 261–272.
- [9] B. Singh, A. Horsewell, P. Toft, *Journal of nuclear materials* 271 (1999) 97–101.
- [10] J. Bryner, *Acta Metallurgica* 14 (1966) 323–336.
- [11] I. Robertson, M. Jenkins, C. English, *Journal of Nuclear Materials* 108 (1982) 209–221.
- [12] L. Horton, J. Bentley, K. Farrell, *Journal of Nuclear Materials* 108 (1982) 222–233.
- [13] T. Takeyama, S. Ohnuki, H. Takahashi, *Trans. Japan Steel Iron Inst.* 21 (1981) 326–331.

- [14] C. Domain, C. Becquart, L. Malerba, *Journal of Nuclear Materials* 335 (2004) 121–145.
- [15] N. Metropolis, A. Rosenbluth, M. Rosenbluth, A. Teller, E. Teller, et al., *The journal of chemical physics* 21 (1953) 1087.
- [16] W. Young, E. Elcock, *Proceedings of the Physical Society* 89 (1966) 735.
- [17] L. Malerba, C. Becquart, C. Domain, *Journal of Nuclear Materials* 360 (2007) 159–169.
- [18] R. Stoller, *Journal of nuclear materials* 233 (1996) 999–1003.
- [19] R. Stoller, G. Odette, B. Wirth, *Journal of Nuclear Materials* 251 (1997) 49–60.
- [20] R. Stoller, A. Calder, *Journal of nuclear materials* 283 (2000) 746–752.
- [21] R. Stoller, *Nuclear engineering and design* 195 (2000) 129–136.
- [22] R. Stoller, S. Guiriec, *Journal of nuclear materials* 329 (2004) 1238–1242.
- [23] R. Stoller, *Journal of nuclear materials* 276 (2000) 22–32.
- [24] M. Finnis, J. Sinclair, *Philosophical Magazine A* 50 (1984) 45–55.
- [25] M. Norgett, et al., *Nuclear Engineering and Design* 33 (1975) 50–54.
- [26] Y. Osetsky, in: *Defect and Diffusion Forum*, volume 188, Trans Tech Publ, pp. 71–92.
- [27] M. Pascuet, N. Castin, C. Becquart, L. Malerba, *Journal of Nuclear Materials* 412 (2011) 106–115.
- [28] N. Castin, M. I. Pascuet, L. Malerba, *Journal of Nuclear Materials* 429 (2012) 315–324.
- [29] F. Nichols, *Journal of Nuclear Materials* 30 (1969) 143–165.
- [30] S. Golubov, R. Stoller, S. Zinkle, A. Ovcharenko, *Journal of Nuclear Materials* 361 (2007) 149–159.
- [31] M. Mendeleev, S. Han, D. Srolovitz, G. Ackland, D. Sun, M. Asta, *Philosophical magazine* 83 (2003) 3977–3994.
- [32] C. Becquart, C. Domain, *Nuclear Instruments and Methods in Physics Research Section B: Beam Interactions with Materials and Atoms* 202 (2003) 44–50.
- [33] C.-C. Fu, J. Dalla Torre, F. Willaime, J.-L. Bocquet, A. Barbu, *Nature materials* 4 (2004) 68–74.
- [34] L. Malerba, M. Marinica, N. Anento, C. Björkas, H. Nguyen, C. Domain, F. Djurabekova, P. Olsson, K. Nordlund, A. Serra, et al., *Journal of Nuclear Materials* 406 (2010) 19–38.
- [35] N. Anento, A. Serra, Y. Osetsky, *Modelling and Simulation in Materials Science and Engineering* 18 (2010) 025008.
- [36] D. Terentyev, L. Malerba, M. Hou, *Physical Review B* 75 (2007) 104108.
- [37] D. Terentyev, T. Klaver, P. Olsson, M. Marinica, F. Willaime, C. Domain, L. Malerba, *Physical Review Letters* 100 (2008) 145503.
- [38] S. Takaki, J. Fuss, H. Kuglers, U. Dedek, H. Schultz, *Radiation Effects and Defects in Solids* 79 (1983) 87–122.
- [39] C. Fu, F. Willaime, P. Ordejón, *Physical review letters* 92 (2004) 175503.
- [40] P. Olsson, 2012. Private communication.
- [41] Y. Fan, A. Kushima, B. Yildiz, *Physical Review B* 81 (2010) 104102.
- [42] K. Arakawa, K. Ono, M. Isshiki, K. Mimura, M. Uchikoshi, H. Mori, *Science* 318 (2007) 956.
- [43] A. Barashev, S. Golubov, H. Trinkaus, *Philosophical Magazine A* 81 (2001) 2515–2532.
- [44] B. Wirth, G. Odette, D. Maroudas, G. Lucas, *Journal of nuclear materials* 276 (2000) 33–40.
- [45] Y. Abe, S. Jitsukawa, *Philosophical Magazine* 89 (2009) 375–388.
- [46] F. Nichols, *Journal of Nuclear Materials* 75 (1978) 32–41.
- [47] D. Terentyev, N. Anento, A. Serra, V. Jansson, H. Khater, G. Bonny, *Journal of Nuclear Materials* 408 (2011) 271–284.
- [48] C. Domain, C. Becquart, J. Foct, *Physical Review B* 69 (2004) 144112.
- [49] C. Först, J. Slycke, K. Van Vliet, S. Yip, *Physical review letters* 96 (2006) 175501.
- [50] C. Becquart, C. Domain, *PERFORM60 report*, 2011.
- [51] N. Anento, A. Serra, *Journal of Nuclear Materials* 440 (2013) 236 – 242.
- [52] G. Lee, J. Kwon, D. Kim, *Nuclear Instruments and Methods in Physics Research Section B: Beam Interactions with Materials and Atoms* 267 (2009) 3214–3217.
- [53] D. Hepburn, G. Ackland, *Physical Review B* 78 (2008) 165115.
- [54] V. Jansson, L. Malerba, *OKMC simulations of Fe-C systems under irradiation: sensitivity studies*, 2013. Submitted to *Journal of Nuclear Materials*.